J|A|C|S
ARTICLES
Published on Web 02/01/2007

Size-Sorted Anionic Iron Oxide Nanomagnets as Colloidal Mediators for Magnetic Hyperthermia

Jean-Paul Fortin,[†] Claire Wilhelm,[†] Jacques Servais,[†] Christine Ménager,[‡] Jean-Claude Bacri,[†] and Florence Gazeau*[,†]

Contribution from the Laboratoire Matière et Systèmes Complexes, UMR CNRS 7057, University Paris 7, 140 rue de Lourmel, 75015 Paris, France, and [2]Laboratoire des Liquides Ioniques et Interfaces Chargées, UMR CNRS 7612, University Paris 6, bât. F, 4 place Jussieu, 75252 Paris, France

Received October 18, 2006; E-mail: floga@ccr.jussieu.fr

Abstract: Iron oxide colloidal nanomagnets generate heat when subjected to an alternating magnetic field. Their heating power, governed by the mechanisms of magnetic energy dissipation for single-domain particles (Brown and Néel relaxations), is highly sensitive to the crystal size, the material, and the solvent properties. This study was designed to distinguish between the contributions of Néel and Brownian mechanisms to heat generation. Anionic nanocrystals of maghemite and cobalt ferrite, differing by their magnetic anisotropy, were chemically synthesized and dispersed in an aqueous suspension by electrostatic stabilization. The particles were size-sorted by successive electrostatic phase separation steps. Parameters governing the efficiency of nanomagnets as heat mediators were varied independently; these comprised the particle size (from 5 to 16.5 nm), the solvent viscosity, magnetic anisotropy, and the magnetic field frequency and amplitude. The measured specific loss powers (SLPs) were in quantitative agreement with the results of a predictive model taking into account both Néel and Brown loss processes and the whole particle size distribution. By varying the carrier fluid viscosity, we found that Brownian friction within the carrier fluid was the main contributor to the heating power of cobalt ferrite particles. In contrast, Néel internal rotation of the magnetic moment accounted for most of the loss power of maghemite particles. Specific loss powers were varied by 3 orders of magnitude with increasing maghemite crystal size (from 4 to 1650 W/g at 700 kHz and 24.8 kA/m). This comprehensive parametric study provides the groundwork for the use of anionic colloidal nanocrystals to generate magnetically induced hyperthermia in various media, including complex systems and biological materials.

Introduction

Colloidal nanocrystals are finding a rapidly increasing number and variety of applications in the biomedical sciences, including detection,[1−3] imaging,[4,5] and therapy.[6,7] These particles have controllable sizes in the nanometer range, on the scale of biological entities, facilitating intimate interactions with cells and molecular constituents. They exhibit remarkable physical properties that can be finely tuned by adjusting the crystal composition, size, and shape.[8,9] This combination of features makes colloidal nanocrystals promising building blocks for advanced bionanotechnologies, based on their optical, magnetic, and electronic properties.

Magnetic nanoparticles are leading candidates for medical applications because of their unique multifunctional properties.[7,10] Indeed, the same magnetic nanocrystal may serve as a contrast agent for magnetic resonance imaging (MRI),[4,11] as a vector for magnetic guidance[12,13] or gene delivery,[14] and also as a nanosource of heat.[15]

As they enhance proton magnetization relaxation at their sites of accumulation, magnetic nanoparticles have been intensively developed for applications in MRI[16] and are now used for diagnostic purposes in clinical practice. They were recently engineered, by conjugation with biomolecules, to target specific

[†] Laboratoire Matière et Systèmes Complexes.
[‡] Laboratoire des Liquides Ioniques et Interfaces Chargées.

(1) Bruchez, M. Jr.; Moronne, M.; Gin, P.; Weiss, S.; Alivisatos, A. P. *Science* **1998**, *281*, 2013−2016.
(2) Dubertret, B. *Med. Sci. (Paris)* **2004**, *20*, 737−740.
(3) Sun, E. Y.; Josephson, L.; Kelly, K. A.; Weissleder, R. *Bioconjugate Chem.* **2006**, *17*, 109−113.
(4) Bulte, J. W.; Kraitchman, D. L. *NMR Biomed.* **2004**, *17*, 484−499.
(5) Michalet, X.; Pinaud, F. F.; Bentolila, L. A.; Tsay, J. M.; Doose, S.; Li, J. J.; Sundaresan, G.; Wu, A. M.; Gambhir, S. S.; Weiss, S. *Science* **2005**, *307*, 538−544.
(6) Couvreur, P.; Vauthier, C. *Pharm. Res.* **2006**, *23*, 1417−1450.
(7) Ito, A.; Shinkai, M.; Honda, H.; Kobayashi, T. *J. Biosci. Bioeng.* **2005**, *100*, 1−11.
(8) Yin, Y.; Alivisatos, A. P. *Nature* **2005**, *437*, 664−670.
(9) Hirsch, L. R.; Gobin, A. M.; Lowery, A. R.; Tam, F.; Drezek, R. A.; Halas, N. J.; West, J. L. *Ann. Biomed. Eng.* **2006**, *34*, 15−22.
(10) Mornet, S. V. S.; Grasset, F.; Duguet, E. *J. Mater. Chem.* **2004**, *14*, 2161−2175.
(11) Weissleder, R. R. P. *Eur. Radiol.* **1993**, *3*, 198−212.
(12) Hafeli, U. O. *Int. J. Pharm.* **2004**, *277*, 19−24.
(13) Fortin-Ripoche, J. P.; Martina, M. S.; Gazeau, F.; Menager, C.; Wilhelm, C.; Bacri, J. C.; Lesieur, S.; Clement, O. *Radiology* **2006**, *239*, 415−424.
(14) Dobson, J. *Gene Ther.* **2006**, *13*, 283−287.
(15) Jordan, A.; Wust, P.; Fahling, H.; John, W.; Hinz, A.; Felix, R. *Int. J. Hyperthermia* **1993**, *9*, 51−68.
(16) Weissleder, R.; Elizondo, G.; Wittenberg, J.; Rabito, C. A.; Bengele, H. H.; Josephson, L. *Radiology* **1990**, *175*, 489−493.

10.1021/ja067457e CCC: $37.00

gene expression[17] or to be internalized by cells and thereby to allow cell migration to be monitored in vivo.[4]

Beyond their potential in medical imaging, nanomagnets can also be used to manipulate labeled entities, as they experience a force when placed in a nonuniform magnetic field.[18] This "action at a distance" opens up many applications involving the transport or immobilization of magnetic nanostructures or magnetically tagged biological entities (including cells) in living organisms. The use of a magnetic driving force is a promising noninvasive strategy for local drug delivery.[13]

The third special property of superparamagnetic nanocrystals, which is the focus of this paper, is their ability to serve as colloidal mediators for heat generation.[15] Single-domain iron oxide nanoparticles possess a global magnetic moment which undergoes orientational thermal fluctuations due to either Brownian fluctuations of the grain itself within the carrier fluid or internal fluctuations of the magnetic moment with respect to the crystal lattice (Néel fluctuations). These fluctuations are responsible for the magnetization relaxation that occurs in a suspension of superparamagnetic particles when the magnetic field is removed. An external AC magnetic field supplies energy that excites the magnetic moment fluctuations, and this magnetic energy is converted into thermal energy. Hence, nanomagnets may serve as nanosources of heat within hybrid nanostructures such as liposomes[19] or inside intimate structures of living organisms, including cells.[20] Magnetically induced hyperthermia has already been used to kill cancer cells after direct intratumoral injection of iron oxide nanoparticles.[21,22] Clinical trials of this method are underway in Germany in patients with brain and prostate cancer.[23]

The unique combination of MRI-based location, magnetic targeting of tumors, and magnetically induced hyperthermia offers interesting possibilities for targeted treatments. Moreover, iron oxide nanoparticles can be combined with thermosensitive drug carriers for controlled drug release.[24]

For magnetic hyperthermia, the most important point is to control the AC field absorption rate, which determines heat generation. The heating power of iron oxide colloidal nanocrystals with diameters above 30 nm is closely dependent on the crystal size, the material, and the solvent properties, which determine the mechanisms of magnetic energy dissipation (Brown and/or Néel relaxation).[25] Here we attempted to distinguish between the contributions of Néel and Brown mechanisms to heat generation. For this purpose, anionic nanoparticles composed of two different materials, cobalt ferrite and maghemite, and with different sizes (range 5−20 nm) were synthesized and dispersed in aqueous solvents of various viscosities. Specific absorption rates were measured systematically as a function of independently varied parameters (particle size distribution, particle material, carrier viscosity, and frequency and amplitude of the external alternating magnetic field). We also made theoretical calculations of heating power and of the respective contributions of relaxation mechanisms, which we then compared with the quantitative experimental data. This parametric study provides the groundwork for the design of colloidal nanocrystals designed to provide magnetically induced hyperthermia in various media, including complex systems and biological materials. Anionic nanomagnets have the major advantage of having a controllable size distribution. We show that, in addition to their use as contrast agents for MRI,[26−28] as biocompatible cell labels,[29−32] and as vectors for magnetic guidance of liposomes,[13] these ion-stabilized, size-sorted iron oxide colloidal nanocrystals can be used for efficient heat generation.

Experimental Methods

Chemical Synthesis. The magnetic dispersions used here were anionic ferrofluids. The ferrite grains were colloidal γ-Fe_2O_3 (maghemite) and $CoFe_2O_4$ (cobalt ferrite) particles chemically synthesized with Massart's procedure[33] by alkaline coprecipitation of iron(III) (1.5 mol) and iron(II) (0.9 mol) (respectively cobalt(II)) salts. After being decantation-sieved, the nanoparticles were suspended in water with 70 g of sodium citrate before heating at 80 °C for 30 min. The particles were washed with acetone and dispersed in water or in a glycerol−water mixture. Colloidal stability was ensured by electrostatic repulsions between the particles due to adsorption of citrate anions to the ferric oxide surface. Colloidal stability was confirmed over a wide temperature range and in external fields up to 800 kA/m, by means of small-angle neutron scattering[34,35] and optical birefringence.[36]

The precursor ferrofluid was size-sorted by a succession of phase separations induced by an increase in ionic strength, i.e., screening of electrostatic repulsions. As the phase diagram is dependent on the particle size, a succession of controlled phase separations was used to reduce polydispersity.[37] Evaporated samples were examined in a JEOL 1200 EX electron microscope.

Magnetization Measurement and Determination of the Particle Size Distribution. The magnetization curves of the nanoparticle suspensions were determined by using a homemade vibrating magnetometer.[38] The magnetization curve $M(H)$ of a suspension of monodisperse iron oxide nanoparticles can be described by a Langevin formalism: $M = m_s\phi(\coth \xi - 1/\xi)$, where $\xi = \mu_0 m_s VH/kT$ is the Langevin parameter, μ_0, the vacuum magnetic permeability, m_s, the

(17) Weissleder, R.; Moore, A.; Mahmood, U.; Bhorade, R.; Benveniste, H.; Chiocca, E. A.; Basilion, J. P. *Nat. Med.* **2000**, *6*, 351−355.
(18) Wilhelm, C.; Gazeau, F.; Bacri, J. C. *Eur. Biophys. J.* **2002**, *31*, 118−125.
(19) Shinkai, M.; Yanase, M.; Honda, H.; Wakabayashi, T.; Yoshida, J.; Kobayashi, T. *Jpn. J. Cancer Res.* **1996**, *87*, 1179−1183.
(20) Jordan, A.; Wust, P.; Scholz, R.; Tesche, B.; Fahling, H.; Mitrovics, T.; Vogl, T.; Cervos-Navarro, J.; Felix, R. *Int. J. Hyperthermia* **1996**, *12*, 705−722.
(21) Jordan, A.; Scholz, R.; Wust, P.; Fahling, H.; Krause, J.; Wlodarczyk, W.; Sander, B.; Vogl, T.; Felix, R. *Int. J. Hyperthermia* **1997**, *13*, 587−605.
(22) Ito, A.; Tanaka, K.; Honda, H.; Abe, S.; Yamaguchi, H.; Kobayashi, T. *J. Biosci. Bioeng.* **2003**, *96*, 364−369.
(23) Maier-Hauff, K.; Rothe, R.; Scholz, R.; Gneveckow, U.; Wust, P.; Thiesen, B.; Feussner, A.; von Deimling, A.; Waldoefner, N.; Felix, R.; Jordan, A. *J. Neurooncol.* **2006**.
(24) Sershen, S.; West, J. *Adv. Drug Delivery Rev.* **2002**, *54*, 1225−1235.
(25) Rosensweig, R. E. *J. Magn. Magn. Mater.* **2002**, *252*, 370−374.
(26) Billotey, C.; Wilhelm, C.; Devaud, M.; Bacri, J. C.; Bittoun, J.; Gazeau, F. *Magn. Reson. Med.* **2003**, *49*, 646−654.
(27) Martina, M. S.; Fortin, J. P.; Menager, C.; Clement, O.; Barratt, G.; Grabielle-Madelmont, C.; Gazeau, F.; Cabuil, V.; Lesieur, S. *J. Am. Chem. Soc.* **2005**, *127*, 10676−10685.
(28) Berret, J. F.; Schonbeck, N.; Gazeau, F.; El Kharrat, D.; Sandre, O.; Vacher, A.; Airiau, M. *J. Am. Chem. Soc.* **2006**, *128*, 1755−1761.
(29) Wilhelm, C.; Gazeau, F.; Roger, J.; Pons, J. N.; Bacri, J. C. *Langmuir* **2002**, *18*, 8148−8155.
(30) Wilhelm, C.; Billotey, C.; Roger, J.; Pons, J. N.; Bacri, J. C.; Gazeau, F. *Biomaterials* **2003**, *24*, 1001−1011.
(31) Riviere, C.; Boudghene, F. P.; Gazeau, F.; Roger, J.; Pons, J. N.; Laissy, J. P.; Allaire, E.; Michel, J. B.; Letourneur, D.; Deux, J. F. *Radiology* **2005**, *235*, 959−967.
(32) Naveau, A.; Smirnov, P.; Menager, C.; Gazeau, F.; Clement, O.; Lafont, A.; Gogly, B. *J. Periodontol.* **2006**, *77*, 238−247.
(33) Massart, R. *IEEE Trans. Magn.* **1981**, *17*, 1247−1248.
(34) Bacri, J.-C. B. F.; Cabuil, V.; Perzynski, R. *Colloids Surf.* **1993**, *A80*, 11−18.
(35) Gazeau, F.; Dubois, E.; Bacri, J.-C.; Boué, F.; Cebers, A.; Perzynski, R. *Phys. Rev. E J1 - PRE* **2002**, *65*, 031403.
(36) Neveu-Prin, S. T. F. A.; Bacri, J. -C.; Perzynski, R. *Colloids Surf.* **1993**, *80*, 1−10.
(37) Massart, R. D. E.; Cabuil, V.; Hasmonay, E. *J. Magn. Magn. Mater.* **1995**, *149*, 1−5.
(38) Bacri, J. C.; Perzynski, R.; Salin, D.; Cabuil, V.; Massart, R. *J. Magn. Magn. Mater.* **1986**, *62*, 36−46.

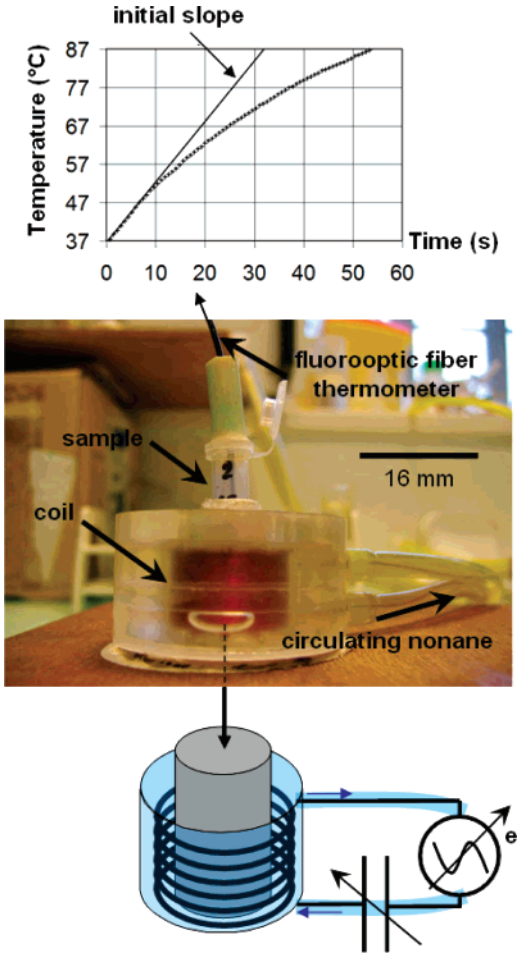

Figure 1. Homemade device for magnetically induced hyperthermia. The ferrofluid sample ($V_s = 300\ \mu$L) is introduced into a copper coil, which is part of a resonant RLC circuit producing an AC magnetic field in the frequency range 300 kHz−1.1 MHz and with amplitudes up to 27 kA/m. The coil is cooled by circulating nonane. Temperature was probed with a fluorooptic fiber thermometer placed in the center of the sample. Example of temperature growth in the ferrofluid (maghemite sample no. 4, $\phi = 0.45\%$). The specific loss power (SLP) was deduced from the initial linear rise in temperature (plain line) versus time, dT/dt, normalized to the mass of magnetic material and the heat capacity of the sample.

saturation magnetization of the magnetic material, H, the magnetic field, k, the Boltzmann constant, T, the temperature, V, the particle magnetic volume, and ϕ, the volume fraction of particles in the suspension. For a polydisperse sample, $M(H)$ was well adjusted by weighting the Langevin expression by a log-normal distribution of particle diameter d,

$$P(d) = \frac{1}{\sqrt{2\pi}\sigma d}\exp\left[-\frac{\ln^2(d/d_0)}{2\sigma^2}\right]$$

The fit of the theoretical expression to the experimental magnetization curve allowed us to determine the characteristic diameter d_0 and the polydispersity index σ for each sample. Standard laboratory-synthesized ferrofluids had a polydispersity index σ of about 0.35−0.4, which could be reduced to 0.2−0.3 after size sorting by successive phase separations.

Experimental Setup for Magnetically Induced Hyperthermia. The homemade device used to induce magnetic hyperthermia is represented in Figure 1. The sample was inserted in a copper coil (diameter 16 mm), which produced an alternating magnetic field in the frequency range 300 kHz−1.1 MHz and with an amplitude of up to 27 kA/m. This coil was an element of a resonant RLC circuit with a variable capacity in the range 10 pF−4 nF and a self-inductance of 25 μH. The coil quality factor was about 75. The sample volume ($V_s = 300\ \mu$L) was chosen to minimize the effects of magnetic field inhomogeneities. To get rid of the influence of thermal gradients arising near the coil, the coil was cooled with circulating nonane. The nonane temperature was tuned in order to obtain an equilibrium temperature of 37 ± 0.5 °C in a 5 mM sodium citrate sample for each amplitude and each frequency of applied magnetic field. Temperature was probed with a fluorooptic fiber thermometer (Luxtron Corp., CA) and was recorded every 0.7 s after switching on the power supply. The initial linear rise in temperature versus time dependence, dT/dt, was measured as illustrated in Figure 1. The specific loss power (SLP) (also called the specific absorption rate) is defined as the thermal power dissipation divided by the mass of magnetic crystal and can be expressed as

$$\mathrm{SLP} = \frac{CV_s}{m}\frac{\mathrm{d}T}{\mathrm{d}t}$$

where C is the volumetric specific heat capacity of the sample, V_s is the sample volume, and $m = \phi\rho V_s$ is the mass of magnetic material in the sample (ρ, the mass per unit volume of iron oxide). For samples in mixed glycerol and water, the C value was defined as the volume-weighted mean of the heat capacities of water and glycerol ($C_{water} = 4185$ J L^{-1} K^{-1}, $C_{glycerol} = 3086$ J L^{-1} K^{-1}).

Theoretical Basis. The heating effects of magnetic nanoparticles submitted to AC magnetic fields are due to several types of loss processes (hysteresis losses, Néel and Brown relaxation), the relative contributions of which depend strongly on particle size. Nanoparticles with a core diameter less than 30 nm, as used here, are single-domain particles. Thus, their magnetization relaxation is governed by the combined effects of the rotational external (Brownian) and internal (Néel) diffusion of the particle magnetic moment.[39] Brown relaxation is due to thermal orientational fluctuations of the grain itself in the carrier fluid, the magnetic moment being locked onto the crystal anisotropy axis. The characteristic time τ_B for Brown relaxation is given by: $\tau_B = 3\eta V_H/kT$, where η is the viscosity of the carrier fluid, k, the Boltzmann constant, T, the temperature, and V_H, the hydrodynamic volume of the particle.

Néel relaxation refers to the internal thermal rotation of the particle's magnetic moment within the crystal, which occurs when the anisotropy energy barrier $E_a = KV$ is overcome; K is the anisotropy constant of the magnetic material, and V is the magnetic particle volume. The characteristic time τ_N for Néel relaxation is written as $\tau_N = \tau_0 \exp(E_a/kT)$, where τ_0 is of the order of 10^{-9} s. As the two relaxation mechanisms take place in parallel, the effective relaxation time τ is given by the relationship: $1/\tau = 1/\tau_N + 1/\tau_B$. Note that the shorter time determines the dominant mechanism of relaxation.

We investigated two iron oxide materials, maghemite and cobalt ferrite, which have magnetic anisotropy constants differing by 2 orders of magnitude[40] in the bulk materials ($K_{\gamma Fe_2O_3} \ll K_{CoFe_2O_4}$). The anisotropy constants of nanoparticles are not precisely known and may have different origins.[41] In the present study, the respective anisotropy constants ($K_{\gamma Fe_2O_3} = 1.6 \times 10^4$ J·m^{-3} and $K_{CoFe_2O_4} = 1.2 \times 10^5$ J·m^{-3}) were deduced, as adjustable parameters, from the fit of experimental SLP data with theory. The hydrodynamic radius was assumed to be 2 nm larger than the magnetic radius. The nanoparticles were dispersed in calibrated mixtures of water and glycerol, with viscosities ranging from $\eta = 7 \times 10^{-4}$ *Pl* to $\eta = 0.33$ *Pl* at 37 °C. Brown and Néel relaxation times, together with the effective time τ, are shown in Figure 2 as a function of the magnetic diameter d, for the extreme values of anisotropy constants (maghemite versus cobalt ferrite particles) and solvent viscosities. The crossover between Néel and Brown regimes of relaxation depends on the anisotropy constant and carrier fluid

(39) Shliomis, M. I. P. A. F.; Morozov, K. I.; Yu, S. I. *J. Magn. Magn. Mater.* **1990**, *85*, 40−46.
(40) Birks, J. B. *Proc. Phys. Soc.* **1950**, *B63*, 65.
(41) Gazeau, F.; Bacri, J.-C.; Gendron, F.; Perzynski, R.; Raikher, Y. L.; Stepanov, V. I.; Dubois, E. *J. Magn. Magn. Mater.* **1998**, *186*, 175−187.

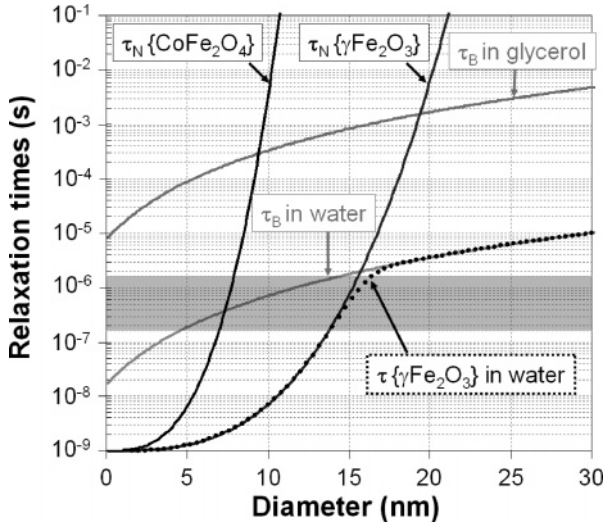

Figure 2. Characteristic times of magnetic moment orientational dynamics as a function of particle diameter. τ_N and τ_B, respectively, characterize the internal fluctuations of the magnetic moment within the crystal (Néel fluctuations) and the Brown fluctuations of the particle within the carrier fluid. The Néel time depends exponentially on magnetic anisotropy and particle volume, whereas Brownian time varies linearly with particle volume and solvent viscosity. Extreme values of characteristic times τ_N and τ_B are displayed: τ_N corresponding to maghemite particles (low magnetic anisotropy) and cobalt ferrite particles (high magnetic anisotropy) and τ_B corresponding to particles in water (low viscosity) and glycerol (high viscosity). The effective relaxation time τ (roughly the shortest time) is represented as a dotted line for maghemite in water. The crossover between Néel and Brownian regimes of relaxation occurs at larger particle sizes with maghemite (16 nm in water and 19 nm in glycerol) than with cobalt ferrite (7.5 nm and 9 nm, respectively). In the range of excitation frequency 100 kHz−1 MHz, fluctuations with characteristic times in the gray zone are preferentially excited and result in heat dissipation.

viscosity. The loss process is governed by Néel relaxation for maghemite particles with diameters below 16 nm in water and 19 nm in glycerol, and below 7.5 and 9 nm, respectively, for cobalt ferrite particles. For larger diameters, losses are mainly due to Brownian relaxation. Note that the Néel relaxation time increases exponentially with the particle volume, whereas the Brownian time increases linearly.

Analytical relationships of power dissipation in a suspension of magnetic nanoparticles have been derived by Rosensweig.[25] Briefly, due to the thermal motion of the particle magnetic moment, the magnetization $\vec{M}$ of the suspension is not in phase with the time-varying magnetic field $\vec{H}$. This phase lag results in conversion of magnetic work $\vec{M}\cdot\vec{H}$ into internal energy. In the framework of a linear response function, $\vec{M} = \chi\vec{H}$, and susceptibility χ is conveniently expressed as a complex number, $\chi = \chi' - i\chi''$, where χ'' is the loss component of susceptibility and represents the portion of magnetization which is in quadrature with the magnetic field. For a number $f = \omega/2\pi$ of field cycles per second, the mean volumetric power dissipation is thus given by $P = \mu_0\pi H_0^2 f\chi''$.

Exponential relaxation of the magnetization with a characteristic time τ is equivalent to a susceptibility expression: $\chi = \chi_0/1 + i\omega\tau$, where χ_0 is the static susceptibility (Debye model). Note that the loss component $\chi'' = \chi_0[(\omega\tau)/(1 + (\omega\tau)^2]$ shows a maximum for $\omega\tau = 1$. Finally, the specific loss power for monodisperse particles is expressed as

$$\mathrm{SLP} = \frac{P}{\rho\phi} = \frac{\mu_0\chi_0 H_0^2}{2\rho\phi}\,\omega\,\frac{\omega\tau}{1+(\omega\tau)^2}$$

In order to take into account the saturation of magnetization with the Langevin parameter ξ, χ_0 was assumed[25] to be the chord susceptibility corresponding to the Langevin equation: $\chi_0 = (\mu_0 m_s^2 \varphi V)/(kT) \times (\coth \xi - 1/\xi)/(\xi)$. Note that the specific loss power is independent of the concentration of magnetic material, is maximum near $\omega\tau = 1$, and, being proportional to $\omega\chi''$, tends toward a plateau for $\omega\tau \gg 1$. Figure 3 shows how SLP varies as a function of the excitation frequency and the particle diameter for maghemite (Figure 3a and 3b) and for cobalt ferrite (Figure 3c and 3d) monodisperse particles. The excitation frequency (in the range 100 kHz-1 MHz) determines the particles with maximal losses, i.e., with $\omega\tau \approx 1$ (1.6×10^{-7} s $< \tau < 1.6 \times 10^{-6}$ s).

The plot of the maghemite SLP as a function of particle size shows a sharp maximum that grows with the frequency and is centered on particle diameters from 16 to 14 nm (Figure 3a). This peak is observed in water as well as in glycerol and can be attributed to internal fluctuations of the magnetic moment (Néel relaxation). The marked dependency of SLP on particle diameter is directly related to the exponential variation of the Néel time with particle volume. A small additional contribution to the SLP is observed in water with particle diameters above 16 nm, but this disappears in glycerol (Figure 3b). This contribution is due to Brownian relaxation and concerns particles with a Néel time longer than the Brownian time.

By contrast, the heating capacity of cobalt ferrite nanoparticles in water results exclusively from rotational friction of the particles within the carrier liquid (Brownian relaxation) for particle diameters above 7.5 nm (Figure 3c, d). The volume dependence of the Brownian time being linear, the SLP profile as a function of particle diameter is rather broad. Nevertheless, a tiny Néel contribution to SLP is observed at small diameters ($d < 7.5$ nm). In glycerol, Brownian relaxation slows down and SLP results solely from Néel relaxation losses, which are efficient, in the frequency range 100 kHz−1 MHz, at diameters between 5 and 9 nm (Figure 3d). Volume being a prefactor in SLP expression, the Néel peak in glycerol is smaller for cobalt ferrite particles than for maghemite, because it occurs at smaller particle diameters.

Given the marked dependency of SLP on particle size, the size distribution in a real sample appears crucial when evaluating the experimental loss power. Figure 4 shows the influence of the polydispersity index on the SLP of maghemite and cobalt ferrite nanoparticles as a function of their characteristic diameter d_0. Like the particle size distribution, the SLP profile becomes smoother as the size dispersion increases. At the same time, the maximum SLP falls drastically in polydisperse maghemite samples. This effect of polydispersity is less pronounced for cobalt ferrite particles due to the broader dependence of monodisperse SLP on particle size (Figure 3c, d).

For comparison with experiments, we derived a theoretical SLP for each sample by taking into account the particle size distribution determined from the magnetization curve.

Results

Table 1 summarizes the different samples used in this study, with their particle and solvent characteristics, and their experimental SLP values at magnetic field amplitude $H = 24.8$ kA/m and frequency $f = 700$ kHz.

Transmission electron micrographs of size-sorted maghemite samples (no. 1−5) are shown in Figure 5a, together with their magnetization curves (Figure 5b) and their size distribution deduced from the fit of magnetization curve (Figure 5c).

Figure 6a shows the kinetics of temperature growth as a function of the field exposure duration for the same maghemite samples as in Figure 5 ($V_s = 300$ μL, $\phi = 0.45\%$, $H = 24.8$ kA/m, $f = 700$ kHz) with particle diameters from 5.3 to 16.5 nm. The initial temperature slope (proportional to the SLP) increased markedly as the particle diameter increased. Note that the SLP (in watts per gram of magnetic material) does not depend on the sample concentration, contrary to the sample equilibrium temperature in a magnetic field. SLP values are

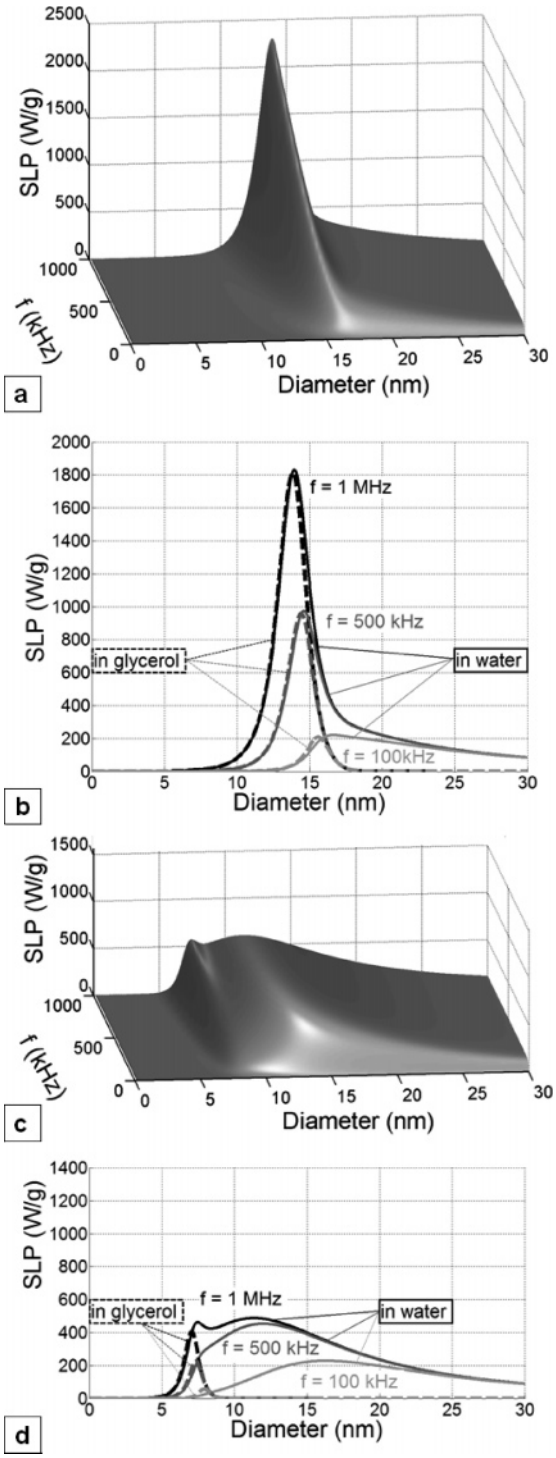

Figure 3. Specific loss power of monodispersed particles of maghemite (a,b) and cobalt ferrite (c,d) as a function of particle diameter and magnetic field frequency. Particles were dispersed in water ((a,c) and (b, d) plain lines) or glycerol ((b,d) dotted lines). The field amplitude was $H = 24.8$ kA/m. Varying the carrier viscosity allowed us to distinguish between the Brownian and Néel contributions to SLP: in glycerol, the Brownian contribution vanishes (Brownian fluctuations are too long to be excited). In water, the SLP is mostly due to Brownian relaxation at particle diameters above 9 nm (cobalt ferrite) and 17 nm (maghemite). The Néel contribution is highly peaked as a function of particle size (at $f = 1$ MHz, it is maximum for 7 nm cobalt ferrite particles and 14 nm maghemite particles) and increased strongly with excitation frequency.

represented in Figure 6b as a function of particle diameter for maghemite (no. 1−5) and cobalt ferrite (no. 6, 7) dispersed in water. For comparison, the calculated SLP values are also shown

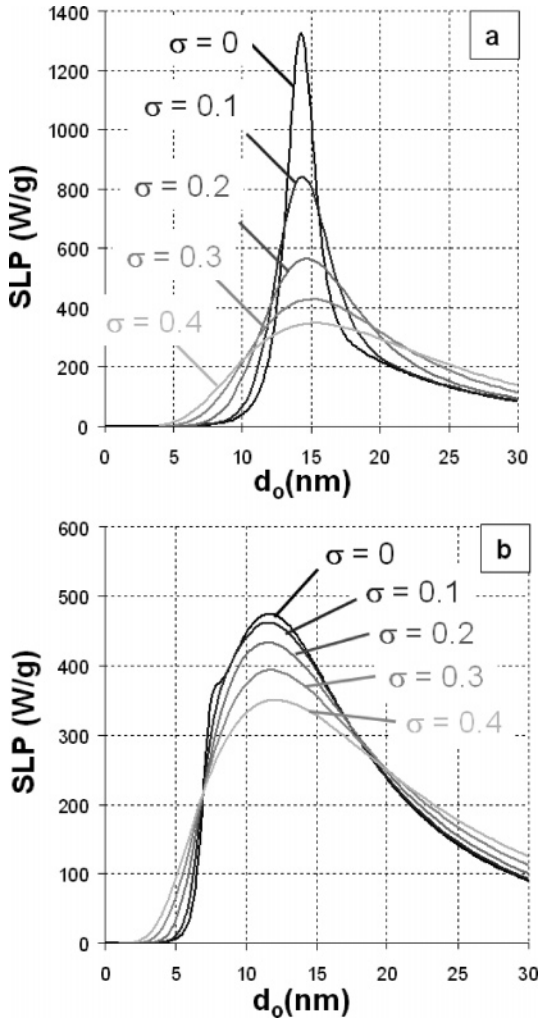

Figure 4. Specific loss power of polydisperse maghemite (a) and cobalt ferrite (b) samples in water as a function of their characteristic diameter d_0 and polydispersity index σ. For maghemite, size dispersion strongly weakens the heating efficiency of samples with characteristic diameters between 12 and 17 nm. The field frequency is 700 kHz and amplitude $H = 24.8$ kA/m.

based on the size distribution and the characteristics shown in Table 1. The SLP of maghemite samples was increased by 3 orders of magnitude (4 to 1650 W/g) for particles with characteristic sizes from 5.3 to 16.5 nm. The theoretical estimates closely fitted the experimental results up to characteristic diameters of 10 nm. For sample no. 5 ($d_0 = 16.3$ nm, $\sigma = 0.43$), the theoretical calculation underestimated the specific loss power. Cobalt ferrite samples (no. 6−7) had higher SLP values than those of maghemite samples of similar size in good agreement with theoretical calculations.

The influence of solvent viscosity is shown in Figure 6c. As expected, the SLP of cobalt ferrite particles diminished drastically with increasing viscosity, in keeping with a predominant contribution of the Brown heating mechanism. Calculated SLPs roughly matched the experimental decay. With maghemite particles the SLPs were only slightly reduced by increasing the solvent viscosity, confirming the predominant contribution of the Néel mechanism of dissipation. The slight decrease in the SLP with viscosity revealed that Brownian mechanisms came into play with the largest maghemite particles in the distribution.

With regard to the magnetic field parameters, the specific loss power varied with the square of the magnetic field

Table 1. Samples Synthesized for This Study, with Their Characteristics and Measured SLP[a]

Sample		1	2	3	4	5	6	7	8	9	10	11	12	13	14	15
Particle material	material	γ-Fe_2O_3					$CoFe_2O_4$		γ-Fe_2O_3				$CoFe_2O_4$			
	m_s (A.m^{-1})	2.8×10^5					3.2×10^5		2.8×10^5				3.2×10^5			
	K (J.m^{-3})	1.6×10^4					1.2×10^5		1.6×10^4				1.2×10^5			
	ρ (kg.m^{-3})	4.9×10^3					5.3×10^3		4.9×10^3				5.3×10^3			
Particle size	d_0 (nm)	5.3	6.7	8.0	10.2	16.5	3.9	9.1	7.1				9.7			
	σ	0.19	0.20	0.21	0.28	0.43	0.4	0.22	0.37				0.35			
Carrier liquid	solvent	water							water and glycerol							
	% glycerol	0							5	30	60	100	5	30	60	100
	η (Pl) x 10^{-3}	0.7							0.75	1.5	5.8	335	0.75	1.5	5.8	335
SLP (W/g)		4	14	37	275	1650	40	360	135	130	125	100	420	220	145	90

[a] Magnetic field amplitude $H = 24.8$ kA·m^{-1} and frequency $f = 700$ kHz.

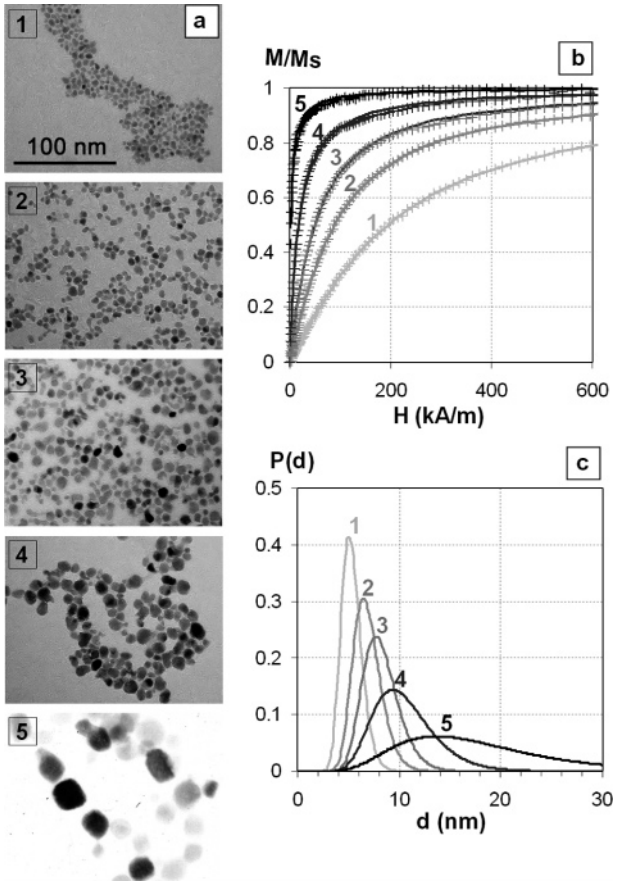

Figure 5. (a) Transmission electron micrographs of size-sorted maghemite samples no. 1−5. (b) Magnetization M of samples no. 1−5 normalized to magnetization saturation M_s as a function of the applied magnetic field is well fitted by Langevin's law weighted by the log normal distribution of particle diameter (solid lines). (c) Size distributions deduced from the fit of magnetization curves for samples no. 1−5. The corresponding characteristic diameters and polydispersity index are indicated in Table 1.

amplitude in all samples (see Figure 7a). The frequency dependency of the SLP in the 300−1100 kHz range differed with the particle size (Figure 7b). The increase was linear with the smallest particles and reached a plateau with the largest particles of both maghemite and cobalt ferrite.

Discussion

It has been known for several years that magnetic nanoparticles are capable of generating much more heat than their micrometric counterparts.[15] The difference lies in intimate magnetic structures. Micrometric magnets possess several magnetic domains, and a magnetic field displaces the domain walls, resulting in a hysteresis loop and energy dissipation. However, wall displacements require a high magnetic field amplitude. By contrast, nanoparticles, being smaller than a domain wall, are single magnetic domains. Each nanoparticle can be considered as a single magnetic moment, the dynamics of which are essentially governed by thermal fluctuations. The two mechanisms of fluctuation of single domains dispersed in a fluid, namely Brown and Néel fluctuations, were reported by Shliomis[39] and Hanson.[42] The physical mechanisms by which magnetic nanoparticles generate heat within an alternating magnetic field have been reviewed by Rosensweig,[25] who underlined the importance of the particle size distribution. However, there are no convincing comparisons of theoretical and experimental heating trends. In particular, there is only indirect evidence distinguishing the Brownian and Néel contributions to heating.[43−45] One difficulty is to obtain samples with a well-characterized size distribution and material characteristics. In this study, we were able to independently vary significant parameters to tune the Brownian time (by varying the viscosity of the suspension medium and the particle size) and the Néel time (by comparing two ferrites with different magnetic anisotropy constants and several particle sizes). A phase separation process to the electrostatically stabilized ionic ferrofluid was performed in order to reduce the size dispersion of the sample and to sort the initially synthesized ferrofluid according to particle size (Figure 5). For each sample, the size distribution deduced by magnetization curve measurement was used in the theoretical model to calculate SLPs for comparison with experimental results.

(42) Hanson, M. *J. Magn. Magn. Mater.* **1991**, *96*, 105−113.
(43) Hiergeist, R. A. W.; Buske, N.; Hergt, R.; Hilger, I.; Richter, U.; Kaiser, W. *J. Magn. Magn. Mater.* **1999**, *201*, 420−422.
(44) Hergt, R. H. R.; Hilger, I.; Kaiser, W. A.; Lapatnikov,Y.; Margel, S.; Richter, U. *J. Magn. Magn. Mater.* **2004**, *270*, 345−357.
(45) Wang, X. G. H.; Yang, Z. *J. Magn. Magn. Mater.* **2005**, *293*, 334−340.

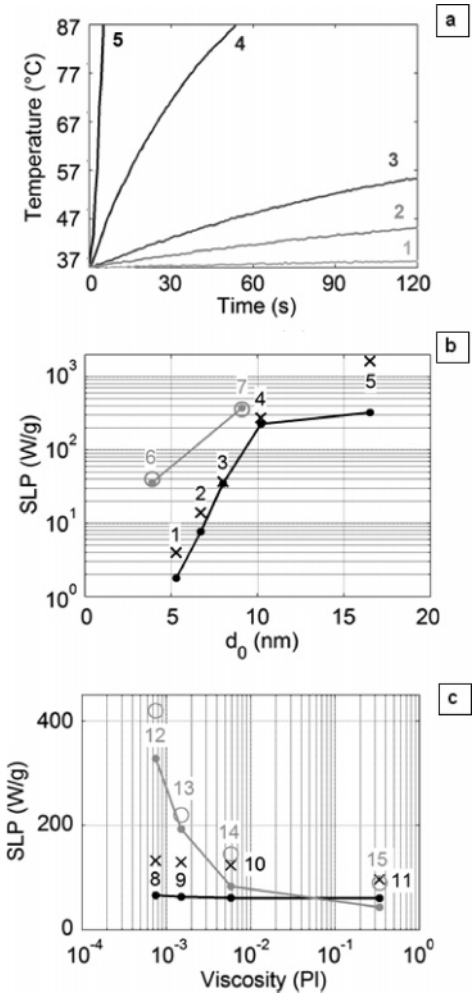

Figure 6. (a) Temperature growth as a function of the field exposure time for maghemite samples no. 1 to 5 with increasing particle diameters from 5.3 to 16.5 nm. The sample concentration is $\phi = 0.45\%$. (b) Specific loss power for maghemite samples no. 1−5 (black cross) and cobalt ferrite samples no. 6 and 7 (gray circles) dispersed in water as a function of their characteristic diameters d_0. For comparison, the SLP values calculated from the size distribution and the characteristics shown in Table 1 are also displayed (solid lines). (c) Influence of carrier fluid viscosity on the SLP of maghemite particles (no. 8−11, $d_0 = 7.1$ nm, $\sigma = 0.37$) (black cross) and cobalt ferrite particles (no. 12−15, $d_0 = 9.7$ nm, $\sigma = 0.35$) (gray circles) dispersed in a mixture of water and glycerol. The experimental SLP for cobalt ferrite declined radically with increasing viscosity, in agreement with the calculated SLP (solid lines). With maghemite, the reduction was small but significant. For all these data the field amplitude was $H = 24.8$ kA/m and the field frequency $f = 700$kHz.

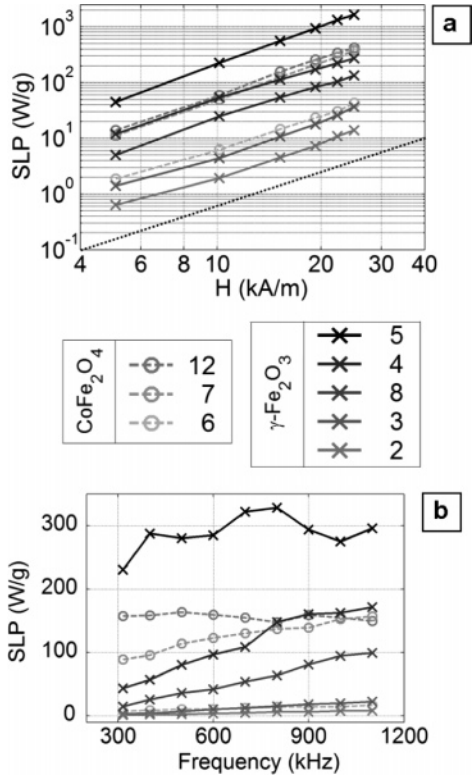

Figure 7. Specific loss power of maghemite samples (no. 2−5 and no. 8 - cross) and cobalt ferrite samples (no. 6, 7, and 12 - circles) as a function of (a) the magnetic field amplitude for a fixed frequency ($f = 700$ kHz) and (b) the magnetic field frequency for a fixed amplitude ($H = 15.2$ kA/m). In the log−log plot of (a), the dashed line (slope = 2) indicates a square dependence of SLP on the field amplitude. The frequency dependence in (b) is a function of particle size: the larger the particles, the more strongly saturated the SLP.

The calculated SLPs shown in Figure 3 clearly distinguish the portions of heat produced by Brown mechanical friction and by Néel internal rotation of the magnetic moment (the Brownian contribution was excluded by using a high-viscosity solvent). Particles with high magnetic anisotropy, such as those composed of cobalt ferrite, dissipate magnetic energy essentially through Brown fluctuations, although with small particles (5−7 nm) Néel fluctuations can be excited in the frequency range used here (100 kHz−1 MHz). As the Brown time increases linearly with particle volume, significant heat arises from Brownian dynamics within a large range of particle diameters (between 5 and 30 nm), and this could be an advantage for polydispersed samples. In contrast, there is an ideal core size for the Néel contribution, yielding a maximum substantial SLP at a given frequency. This strong size dependency arises from exponential growth of the Néel time with the anisotropy energy (the anisotropy constant multiplied by the particle volume). At frequencies from 100 kHz to 1 MHz, the ideal size varies within a narrow range of 16−14 nm for maghemite (7−6 nm for cobalt ferrite). Experimental SLPs depend on the overlap between the size distribution and the SLP profiles in Figure 3. Very substantial heating can be achieved by Néel relaxation when the size distribution approaches the SLP profile.

This theory, taking into account the entire size distribution, gives estimates that correspond to quantitative experimental results predicting the dependency of SLP values on size (Figure 6b), magnetic anisotropy (Figure 6b), and the viscosity of the medium (Figure 6c).

Without size sorting, a standard anionic maghemite ferrofluid (sample no. 8: $d_0 = 7.1$ nm, $\sigma = 0.37$) has an SLP of 135 W/g at 24.8 kA/m and 700 kHz. In contrast, the SLPs of the four size-selected samples (no. 1−4) with reduced polydispersity ranged from 4 to 275 W/g, in good agreement with theoretical values. Hergt et al.[46] obtained similar results after magnetic separation of Dextran-coated particles.

Maghemite particles (sample no. 5) with a characteristic size of 16.5 nm and a large size distribution yielded the most efficient heat generation, with an SLP of 1650 W/g at 24.8 kA/m (or 300 W/g at 11 kA/m). Although not easy with large particles,

(46) Hergt, R. H. R.; Zeisberger, M.; Glöckl, G.; Weitschies, W.; Ramirez, L. P.; Hilger, I.; Kaiser, W. A. *J. Magn. Magn. Mater.* **2004**, *280*, 358−368.

this sample could be size-sorted to further improve the SLP. For comparison, the maximum SLP values reported in the literature[10] were obtained with Dextran-coated magnetite particles[47] (up to 400 W/g at 8 kA/m and 1 MHz, with a pronounced Dextran molecular weight-related increase in the SLP), for 15.3-nm particles coated with polyethylene glycol[44] (600 W/g for 11 kH/m and 400 kHz) and for bacterial magnetosomes[48] of a 20−45 nm core diameter (960 W/g at 10kA/m and 410 kHz). It is noteworthy that experimental values for particles of 15 nm and larger were higher than theoretically predicted. The limits of the model based on the superparamagnetic behavior of a single domain may thus be reached in these conditions. The magnetic anisotropy of large particles may be modified owing to changes in particle shape. Moreover, the spatial organization of the particles (for example, chain formation by bacterial magnetosomes) may influence heating capacity, as magnetic interactions may perturb both Brownian and Néel relaxation. The stability of the colloidal suspension is also critical for reliable calorimetric measurement.

As predicted theoretically, cobalt ferrite particles with a characteristic size below 10 nm had SLP values in water (up to 420 W/g at 24.8 kA/m) higher than those of maghemite particles of comparable size (Figure 6). Our data therefore show that cobalt ferrite particles are suited to heat generation, even though a large part of the heat they generate arises from Brownian mechanical friction.

As regards the magnetic field parameters, the square dependence of SLP on the field amplitude (Figure 7) was shown to hold up to 24.8 kA/m for all samples, in agreement with previous studies.[43,46] Two patterns of frequency dependence were observed (Figure 7b): SLP increased linearly with frequency for samples of characteristic diameter below 10 nm and saturated with larger particles. The frequency dependence was less pronounced for cobalt ferrite (consistent with Brownian relaxation) than for maghemite particles. Note that the size dispersion of experimental samples strongly attenuates the theoretical frequency-related increase in the contribution of the Néel phenomenon.

The effect of solvent viscosity was clearly shown by using a mixture of water and glycerol. In contrast with other studies using sol−gel transition,[43] we varied the viscosity and specific heat capacity of the samples continuously, and the stability of the colloidal dispersion was preserved. A 500-fold variation of viscosity allowed us to measure the Brown contribution to the absorption rate. In agreement with theory, the SLP diminished as viscosity increased, the effect being more pronounced with cobalt ferrite (420 to 90 W/g) than with maghemite (135 to 100 W/g). This showed that the magnetic heating rate was mainly due to Brown fluctuations with the cobalt ferrite sample and to Néel relaxation with the maghemite sample. It also revealed a subsidiary contribution of Brownian relaxation to the maghemite SLP, probably owing to the largest particles in the distribution. Conversely, Néel losses due to the presence of small particles were responsible for about one-quarter of the cobalt ferrite SLP.

These results have important implications for the control of magnetically induced heating in complex media, including body tissues and fluids. As the dynamics of magnetic nanoparticles are sensitive to their local microenvironment, the heating power of nanoparticles embedded in complex structures such as cell endosomes[49] or drug reservoirs[27] may be modified relative to the initial colloid.

Other mechanisms have been implicated in the sensitivity to the local microenvironment of iron oxide nanoparticles used as contrast agents for MRI.[26,27] Here we highlight the role of local viscosity (or restriction of particle orientation) on the specific loss power of different nanoparticles. This could help guide the choice of particles for specific applications (cell or tissue hyperthermia, thermally monitored drug release, etc.).

To conclude, anionic iron oxide nanoparticles appear to be versatile mediators of magnetic hyperthermia in various media. Through electrostatic interactions, anionic citrated nanoparticles can readily be associated with various complex structures. By electrostatic self-assembly with charged copolymers, they can form controlled hybrid aggregates,[28] which are building blocks for biological functionalization and targeting. These nanoparticles have also been entrapped in nanosized pegylated liposomes[27] and then successfully guided by magnetic force to a solid tumor in a mouse model.[13] As liposomes can also act as drug vehicles, magnetic hyperthermia could be combined with chemotherapy for a synergic therapeutic effect at the tumor site. Moreover, magnetic nanocomposites open new possibilities for magnetically induced drug release.

Anionic magnetic nanoparticles have shown their affinity for biological cells.[29] Without the need for transfection agents or additional coatings, negatively charged citrated nanoparticles are spontaneously adsorbed to the cell membrane and then internalized into cell endosomes, much more efficiently than Dextran-coated particles[30] and with no toxicity.[31,32] The possibilities of intracellular hyperthermia with such anionic particles will be examined in a forthcoming paper.

Conclusion

We investigated the potential of iron oxide nanomagnets with well-characterized particle size distributions, magnetic anisotropy, and carrier fluids for their efficiency as heat mediators. We performed a parametric study in which we independently varied parameters relevant to Brownian and Néel loss mechanisms, for both theoretical predictions and measured data. For a more meaningful comparison with experimental data, the actual size distribution of each sample was introduced in the model. To our knowledge, this is the first time that quantitative magnetic hyperthermia data have been shown to concord with theoretical predictions based on relevant parameters (particle size and material, viscosity, field characteristics). This allowed us to clearly distinguish the respective inputs of the different relaxation mechanisms and to predict the behavior of such biocompatible anionic nanomagnets in complex media.

Acknowledgment. We thank S. Neveu for providing us with the cobalt ferrite particles and D. Talbot for technical assistance. We also thank M. Devaud for fruitful discussions. This work was supported by the Centre National de la Recherche Scientifique and the Ministère de la Recherche (ACI Nanoscience et Nanotechnologie NR0145).

JA067457E

(47) Chan, D. C. F. K. D. B.; Bunn, P. A. In *Scientific and Clinical Applications of Magnetic Carriers*; Häfeli, U., Teller, W. S. J., Zborowski, M., Eds.; Plenum Press: New York, 1997; p 607.
(48) Hergt, R. H. R.; Zeisberger, M.; Schüler, D.; Heyen, U.; Hilger, I.; Kaiser, W. A. *J. Magn. Magn. Mater.* **2005**, *293*, 80−86.
(49) Wilhelm, C.; Cebers, A.; Bacri, J. C.; Gazeau, F. *Eur. Biophys. J.* **2003**, *32*, 655−660.